Discovery of the galaxy counterpart of HDF 850.1, the brightest submillimetre source in the *Hubble Deep Field*

J. S. Dunlop,[1]* R. J. McLure,[1] T. Yamada,[2] M. Kajisawa,[2] J. A. Peacock,[1] R. G. Mann,[1] D. H. Hughes,[3] I. Aretxaga,[3] T. W. B. Muxlow,[4] A. M. S. Richards,[4] M. Dickinson,[5] R. J. Ivison,[6] G. P. Smith,[7] I. Smail,[7] S. Serjeant,[8] O. Almaini[1] and A. Lawrence[1]

[1]*Institute for Astronomy, University of Edinburgh, Royal Observatory, Blackford Hill, Edinburgh EH9 3HJ*
[2]*National Astronomical Observatory, 2-21-1, Osawa, Mitaka, Tokyo 181-8588, Japan*
[3]*Instituto Nacional de Astrofísica, Óptica y Electrónica (INAOE), Apartado Postal 51 y 216, 72000 Puebla, Pue., Mexico*
[4]*University of Manchester, MERLIN/VLBI National Facility, Jodrell Bank Observatory, Cheshire SK11 9DL*
[5]*Space Telescope Science Institute, Baltimore, MD 21218, USA*
[6]*UK ATC, Royal Observatory, Blackford Hill, Edinburgh EH9 3HJ*
[7]*Department of Physics, University of Durham, South Road Durham DH1 3LE*
[8]*Centre for Astrophysics & Planetary Science, School of Physical Sciences, University of Kent, Canterbury CT2 7NZ*

ABSTRACT

Despite extensive observational efforts, a convincing optical/infrared identification of the brightest submm source in the *Hubble Deep Field*, HDF 850.1, has remained elusive after almost four years. This failure is all the more notable given the availability of supporting multifrequency data of unparalleled depth, and subarcsec positional accuracy for the submm/mm source. Consequently, HDF 850.1 has become a test case for the possibility that the most violently star-forming objects in the Universe are too red and/or distant to be seen in the deepest optical images.

Here we report the discovery of the galaxy counterpart of HDF 850.1. This object has been revealed by careful analysis of a new, deep K' image of the HDF obtained with the Subaru 8.2-m telescope. Its reality is confirmed by a similar analysis of the *HST* NICMOS F160W image of the same region. This object is extremely faint ($K \simeq 23.5$), clumpy (on subarcsec scales) and very red ($I - K > 5.2$; $H - K = 1.4 \pm 0.35$). The likelihood that it is the correct galaxy counterpart is strongly reinforced by a reanalysis of the combined MERLIN+VLA 1.4-GHz map of the field, which provides a new radio detection of HDF 850.1 only 0.1 arcsec from the new near-infrared counterpart, and with sufficient positional accuracy to exclude all previously considered alternative optical candidates.

We have calculated new confidence limits on the estimated redshift of HDF 850.1 in the light of the new radio detection, and find $z = 4.1 \pm 0.5$. We have also determined the scalelength, and hence estimated the mass of the apparently nearby (0.5 arcsec distant) $z \simeq 1$ elliptical galaxy $3-586.0$. From this we calculate that the flux density of HDF 850.1 has been boosted by a factor of $\simeq 3$ through gravitational lensing by this intervening elliptical, consistent with predictions that a small but significant fraction of blank-field submm sources are lensed by foreground galaxies. We discuss the wider implications of these results for the submm population and cosmic star formation history.

Key words: galaxies: evolution – galaxies: formation – galaxies: starburst – cosmology: observations – infrared: galaxies.

*E-mail: jsd@roe.ac.uk
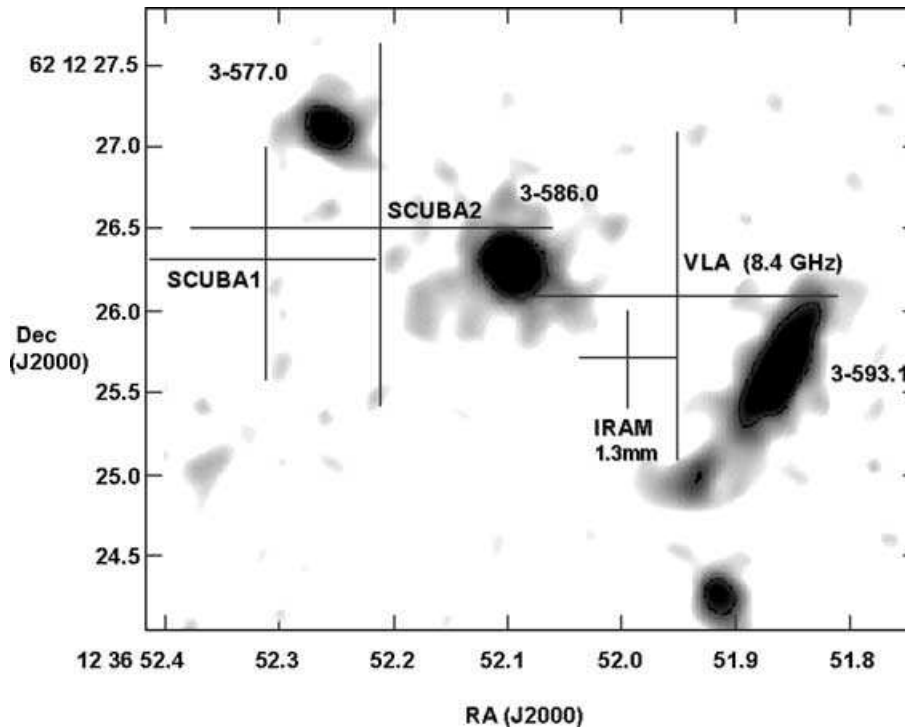
Figure 1. Positional information on HDF 850.1 available prior to the current study. Superimposed on a grey-scale of the WFPC2 optical image of the relevant region are: (i) the original position of the SCUBA 850 μm source HDF 850.1 reported by Hughes et al. (1998) (marked SCUBA1); (ii) the revised position of the 850 μm detection deduced by Serjeant et al. (2002) (marked SCUBA2); (iii) the position of the tentative 8.4-GHz detection VLA 3651+1226 reported by Richards et al. (1998); and (iv) the position of the 1.3-mm detection with the IRAM PdB interferometer reported by Downes et al. (1999). In each case the size of the cross indicates the 1σ error in the relevant position (see Section 2 for further details).

1 INTRODUCTION

HDF 850.1 was the first submm source discovered via unbiased, blank-field surveys at 850 μm, its presence becoming apparent only $\simeq$15 h into the 50-h SCUBA imaging observation of the *Hubble Deep Field* (HDF) undertaken by Hughes et al. (1998). It was also the first SCUBA-selected source to be detected in continuum emission through mm-wavelength interferometry, with $\simeq$40 h of observations with the IRAM PdB interferometer yielding its position to an accuracy of ±0.3 arcsec (Downes et al. 1999). Frustratingly, however, despite this accurate position and the obvious availability of optical data of unparalleled depth and resolution, a convincing galaxy counterpart for this bright submm source has not yet been identified. Indeed, the difficulty experienced in finding an optical counterpart for HDF 850.1 has even motivated some authors to explore the possibility that some of the submm sources uncovered via high-galactic-latitude SCUBA surveys are actually galactic objects (Lawrence 2001).

It is important to note, however, that, even though the search radius permitted by the IRAM PdB results is small, this failure of identification is *not* due to a lack of potential optical counterparts (see Fig. 1). Indeed, both Hughes et al. (1998) and Downes et al. (1999) noted that the galaxy 3−586.0, one of the most obviously red objects in the three-colour image of the HDF, is not only consistent with the mm/submm position of HDF 850.1, but is statistically unlikely to lie so close to the submm/mm source by chance ($p \simeq 0.05$, because 3−586.0 is relatively bright). Both Hughes et al. (1998) and Downes et al. (1999), however, rejected the possibility that this apparently favourable statistical association necessarily implies that 3−586.0 is the correct optical identification. This is because, while optical–

near-infrared photometry of 3−586.0 strongly indicates that it is a passively evolving elliptical at $z \simeq 1$ (Fernández-Soto, Lanzetta & Yahil 1999; Rowan-Robinson 2003), existing submm to radio detections and limits yield an estimated redshift (z_{est}) for the 850 μm source of $z_{est} \simeq 4$, and appear to exclude $z < 2$ (e.g. Carilli & Yun 1999; 2000; Dunne, Clements & Eales 2000). Furthermore, as argued by Downes et al. (1999), it is not expected that such a quiescent elliptical should be a strong emitter of submm radiation.

Consequently, HDF 850.1 has become the classic test case of the extent to which the technique of estimating redshifts from submm to radio photometry can be trusted, and indeed of the whole idea that many/most bright submm sources lie at high redshift ($z > 2$).

Given the apparent unsuitability of 3−586.0, the two remaining potential high-redshift objects in the vicinity of HDF 850.1 have both been considered as potential identifications. First, Hughes et al. (1998) tentatively suggested 3−577.0 as the correct identification because, while statistically quite likely to lie close to the submm position by chance ($p \simeq 0.3$), it appeared to be the only candidate within the SCUBA search radius with a photometric redshift (z_{ph}) in the appropriate range ($z_{ph} \simeq 2.9$, Fernández-Soto et al. 1999; Rowan-Robinson 2003; and a tentative spectroscopic redshift $z_{sp} = 3.36$, Zepf, Moustakas & Davis 1997). Subsequently, the improved IRAM PdB position excluded this object as a possible counterpart, and Downes et al. (1999) concluded in favour of 3−593.1. However, the relatively modest photometric redshift of this source ($z_{ph} \simeq 1.75$, Fernández-Soto et al. 1999; Rowan-Robinson 2003) means that this option also appears unconvincing.

One might reasonably ask why the correct optical/infrared identification for HDF 850.1 has proved so elusive, given that several other comparably bright submm sources have been discovered and

unambiguously identified in the intervening years (e.g. Smail et al. 1999; Ivison et al. 1998, 2000; Gear et al. 2000; Frayer et al. 2000; Lutz et al. 2001). The most likely explanation is simply that HDF 850.1 lies at a more extreme redshift than these identified sources, which generally have estimated redshifts $z_{est} < 3$. The strongest hint of this comes from the fact that these identified SCUBA sources have been detected in the radio at $S_{1.4GHz} > 50 \, \mu$Jy, whereas HDF 850.1 has evaded radio detection at the level of $S_{1.4GHz} < 23 \, \mu$Jy (3σ).

The radio investigation of HDF 850.1 was temporarily confused by the suggestion of Richards (1999) that the submm source should be associated with the radio source VLA 3651+1221, some 6 arcsec south-west of the SCUBA position. This possibility was excluded shortly thereafter by the IRAM PdB detection. However, this diversion does at least serve to emphasize the dangers of making the (initially understandable) assumption that every SCUBA source can be reliably associated with a VLA source provided one is found within a fairly generous search radius (e.g. Barger, Cowie & Richards 2000), and confirms that any redshift distribution for the submm population deduced from such SCUBA+VLA associations should be regarded as conservative (as noted by Smail et al. 2000). In fact, to date the most promising radio counterpart of HDF 850.1 is VLA 3651+1226, listed in the supplementary list of sources provided by Richards et al. (1998) as a 2.3σ detection at 8.4 GHz. Subsequent reanalysis of these data has raised the significance of this detection to over 3σ, with $S_{8.4GHz} = 7 \, \mu$Jy. However, even if real, this 8.4-GHz detection is still consistent with the 1.4-GHz limit, and the fact that the observed radio flux density from HDF 850.1 is lower than that of comparably bright submm sources that have already been successfully identified.

In this paper we report new results which reveal the galaxy counterpart of HDF 850.1 to be a faint, extremely red object lying at $z_{est} \simeq 4$. This conclusion follows from a detailed analysis of a new, deep ($>$10-h), high-quality (0.6-arcsec seeing) K' image of the HDF obtained with the 8.2-m Subaru telescope. This has revealed a new near-infrared counterpart to HDF 850.1, which we also find to be marginally detected in the *HST* NICMOS F160W image of the HDF. Our conclusion that this new, faint, red object is indeed the galaxy counterpart of the submm source is then strengthened by a reanalysis of the combined MERLIN+VLA 1.4-GHz radio image of the HDF. This yields a 4σ detection of HDF 850.1 only 0.1 arcsec distant from the new near-infrared counterpart, and with sufficient positional accuracy to exclude all the previously considered alternative optical candidates discussed above. We have also utilized this new radio detection in a calculation designed to set realistic confidence limits on the estimated redshift of HDF 850.1, and find $z_{est} = 4.1 \pm 0.5$. Finally, since this new discovery cannot change the fact that the $z \simeq 1$ elliptical 3−586.0 is unlikely to lie so close to the submm/mm/radio source by chance, we calculate the probability of the most likely explanation of this coincidence, namely that HDF 850.1 is gravitationally lensed by 3−586.0. This possibility has been considered before by Hughes et al. (1998) and Downes et al. (1999) (and indeed a lensing model for 3−586.0 was discussed by Hogg et al. (1996) prior to the discovery of HDF 850.1). However, a more accurate calculation can now be performed, given the improved positional accuracy for HDF 850.1, new limits on the brightness of a counter image, and the accurate estimate of the mass of 3−586.0 that we have deduced from our detailed modelling of the infrared and optical images.

The structure of the paper is as follows. In the next section we briefly summarize all the multifrequency information for HDF 850.1 (and its immediate vicinity) that was available prior to this new study. Then, in Section 3 we describe the new K' data, and the re-

sults of the reanalysis of the MERLIN+VLA 1.4-GHz data set. In Section 4 we explain how we analysed the K' image in two independent ways, and demonstrate that both methods reveal the same new candidate identification, which we hereafter refer to as HDF 850.1K. We also show that a similar analysis of the existing *HST* NICMOS F160W image of the HDF yields a marginal *H*-band detection of this object.

In Section 5 we present photometric and astrometric information for HDF 850.1K, summarize the properties of the elliptical 3−586.0 derived from our image analysis, and present new confidence limits on the estimated redshift of HDF 850.1. In Section 6 we draw this information together and provide a quantitative discussion of the likelihood that the new near-infrared identification is indeed the galaxy counterpart of HDF 850.1. We also calculate the likely extent to which this source has been gravitationally lensed by the elliptical 3−586.0. We conclude with a discussion of the implications of these new results for the submm galaxy population in general, and for current estimates of star-formation density at high redshift. Throughout this paper we assume a flat cosmology with $H_0 = 70 \, \text{km} \, \text{s}^{-1} \, \text{Mpc}^{-1}$, $\Omega_m = 0.3$, and $\Omega_\Lambda = 0.7$.

2 EXISTING DATA

2.1 Submillimetre data

HDF 850.1 was detected by Hughes et al. (1998) at 850 μm with a flux density of $S_{850\mu m} = 7.0 \pm 0.5$ mJy. This flux density, derived from the map, was also confirmed to within the errors by pointed photometric observations. The position of this object as derived from the original SCUBA map of the HDF was (J2000)

RA $12^h \, 36^m \, 52^s.32$, Dec $+ 62° \, 12' \, 26''.3$.

The formal uncertainty in this position, based on the SCUBA beam size at 850 μm, and the signal-to-noise ratio of the detection was quoted by Hughes et al. (1998) to be 0.7 arcsec (1σ) in each dimension. This position, along with the 1σ errors, is marked by a cross in Fig. 1, and labelled 'SCUBA1'.

A reanalysis of the HDF SCUBA map has recently been completed by Serjeant et al. (2003), using the maximum-likelihood source extraction technique described by Scott et al. (2002). This yields a slightly different position for HDF 850.1 (albeit one consistent with the originally quoted formal uncertainty), namely (J2000):

RA $12^h \, 36^m \, 52^s.22$, Dec $+ 62° \, 12' \, 26''.5$.

Serjeant et al. (2002) also performed a series of simulations to estimate the effect of confusion noise on extracted source position in the SCUBA HDF map, and found that, even at the 7 mJy level, the mean positional offset is $\simeq$1.5 arcsec. In Fig. 1 we therefore also show this revised SCUBA position for HDF 850.1, labelled 'SCUBA2', with a positional error of 1.5 arcsec (1.1 arcsec in each dimension).

Hughes et al. (1998) also derived a 450-μm 3σ upper limit of $S_{450\mu m} < 21$ mJy. As discussed by these authors, a non-detection at this level constrains the redshift of HDF 850.1 to $z_{est} > 2.5$, for the known range of far-infrared-to-submm spectral energy distributions.

Finally, we note that Serjeant et al. (2003) quote a somewhat smaller value for the 850 μm flux density (i.e. $S_{850\mu m} = 5.6 \pm 0.4$ mJy) of HDF 850.1. However, in this paper we adopt the originally quoted value of 7 mJy, because this value is more consistent with the result derived from the pointed photometric observations ($S_{850\mu m} = 7.0 \pm 0.4$ mJy; Hughes et al. 1998).

2.2 Millimetre data

HDF 850.1 was also detected by Hughes et al. (1998) at 1.35 mm, and found to have a flux density of $S_{1.35\,mm} = 2.1 \pm 0.5$ mJy. This observation was made with a beam of FWHM 23 arcsec, and so can safely be regarded as a measure of the total 1.35 mm flux density of the source. Given this, the subsequent measurement of $S_{1.3\,mm} = 2.2 \pm 0.3$ mJy by Downes et al. (1999) within the $\simeq 2$-arcsec beam of the IRAM PdB interferometer indicates that the source is reasonably compact.

The 1.3-mm position measured for HDF 850.1 by Downes et al. (1999) is (J2000)

RA 12^h 36^m $51^s.98$, Dec $+ 62° 12' 25''.7$,

with an uncertainty of 0.3 arcsec (1σ) in each dimension. This position, along with the 1σ errors, is marked by a cross labelled 'IRAM 1.3mm' in Fig. 1. This position is clearly consistent with the SCUBA position in the light of the revised uncertainty in the SCUBA astrometry discussed above. It is 1.9 arcsec distant from the SCUBA position of HDF 850.1 derived by Serjeant et al. (2003), corresponding to the 69th percentile of the distributions of positional offsets estimated from the simulations of the effects of confusion noise on source position.

2.3 Radio data

The formal position of the only possible marginal radio detection of HDF 850.1 (i.e. the $\simeq 3\sigma$ $S_{8.4\,GHz} \simeq 7$ μJy 'source' VLA 3651+1226 from the supplementary list of sources in Richards et al. 1998) is (J2000)

$RA\,12^h 36^m 51^s.96$, Dec $+ 62° 12' 26''.1$,

but the low significance of this detection means that the 1σ error in this position is $\simeq 1$ arcsec in each dimension. This position, and the 1σ errors, is marked by the large cross labelled 'VLA 8.4GHz' in Fig. 1. It can be seen that the position of this radio detection is consistent with both the SCUBA and IRAM positions.

2.4 Optical data

Finally, also shown (and labelled) in Fig. 1 are the three optical objects 3−577.0, 3−586.0, and 3−593.1 which, as discussed in the Introduction, have been previously considered as potential identifications by various authors. Unfortunately, a spectroscopic redshift has yet to be determined for any of these objects, despite, at least in the case of 3−586.0, deep optical spectroscopy with the 10-m Keck telescope (Stern, private communication). The colour-estimated redshifts for these three objects are $z_{ph} \simeq 2.9$, $z_{ph} \simeq 1.1$ and $z_{ph} \simeq 1.7$ respectively (Fernández-Soto et al. 1999; Rowan-Robinson 2003). In the case of 3−586.0, the photometric redshift is relatively secure due to the fact that its broad-band spectral energy distribution (SED) so clearly mimics that expected from an evolved elliptical at $z_{ph} \simeq 1$, with a clear break between the I and J bands. The apparent passivity of this elliptical is also the most likely explanation for the lack of any discernable emission-line features in its optical spectrum.

The positions of the optically detected galaxies shown in Fig. 1 are as given in Williams et al. (1996) and Downes et al. (1999). However, the ±0.4-arcsec errors on RA and Dec given in these papers can now be revised down to ±0.1 arcsec following the registration of the HDF optical image with the MERLIN image (see Section 3.2) to within an accuracy of 50 mas.

3 NEW OBSERVATIONS

3.1 Deep Subaru K' Imaging

The new deep K' image of the HDF-N was obtained with the Subaru 8.2-m telescope equipped with the NIR camera CISCO (Motohara et al. 2002) on 2001 April 3–4. Full details of the observations and data reduction will be given in a future publication (Kajisawa et al., in preparation). Here we briefly summarize the data properties. The net on-source integration time is 10.2 h. The data were reduced in a standard manner; each individual frame was flat-fielded and median-sky subtracted before the frames were combined. Photometric calibration was performed using UKIRT Faint Standard Stars observed at various altitudes during the observation, to produce K magnitudes in the UKIRT Mauna Kea system (Hawarden et al. 2001). We have ignored the $K' \rightarrow K$ colour correction, which introduces an uncertainty in the K magnitude of the detected sources of at most 0.1 mag depending on their spectra. The original pixel scale of CISCO is 0.111 arcsec, but the images have been carefully resampled to match the WFPC2 drizzled data (see Subsection 4.1 below). The seeing was 0.4–0.6 arcsec during the observations, and the FWHM of stellar objects in the final image is $\simeq 0.6$ arcsec. The peak of the number counts of the detected sources reaches a magnitude of $K \simeq 23$. A grey-scale representation of the 8×8 arcsec^2 subregion of this image, centred on 3−586.0, is shown in the top panels of Fig. 2.

3.2 MERLIN+VLA 1.4-GHz image

A total of 18 d of MERLIN data and 42 h of A-array VLA data at 1.4 GHz have been combined to image radio sources in a 10-arcmin field centred on the HDF. This area includes both the HDF and the Hubble Flanking Fields (HFF). These are the most sensitive 1.4-GHz images yet made, with rms noise levels of 3.3 μJy beam^{-1} in the 0.2-arcsec resolution images (Muxlow et al., in preparation). Positions derived from the independent MERLIN and VLA imaging are with respect to the International Celestial Reference Frame (ICRF, Ma et al. 1998), and agree to better than 15 mas over the entire 10 arcmin field. Radio sources associated with compact galaxies have been used to align the *HST* WFPC2 optical fields to better than 50 mas in the HDF itself, and to better than $\simeq 150$ mas in the outer parts of the HFF (Muxlow et al. 2000). This astrometric alignment of the *HST* WFPC2 fields has been used by Garrington, Muxlow & Garrett (2000) to argue that the position of HDF 850.1 as measured by the IRAM telescope (Downes et al. 1999), again with respect to the ICRF, precludes its identification with any galaxy visible on the HDF WFPC2 frame.

In that region of the HDF close to the position of HDF 850.1, the high-resolution MERLIN+VLA image has been smoothed to 0.6-arcsec resolution. In the smoothed image, an area of extended radio emission is detected between the elliptical galaxy 3−586.0 and the IRAM position for HDF 850.1. This detection is shown by the contours in the upper panel of Fig. 4, where it can be seen that the radio emission splits roughly into two components, one partially overlaying the central region of 3−586.0, and the other lying 0.5 arcsec to the east of the IRAM position. Fitting a two-dimensional Gaussian to the latter radio component yields a flux of 16 μJy at the position given in Table 2. With an rms noise level of 3.7 μJy beam^{-1} in the smoothed radio image, the source detection is significant at better than the 4σ level.
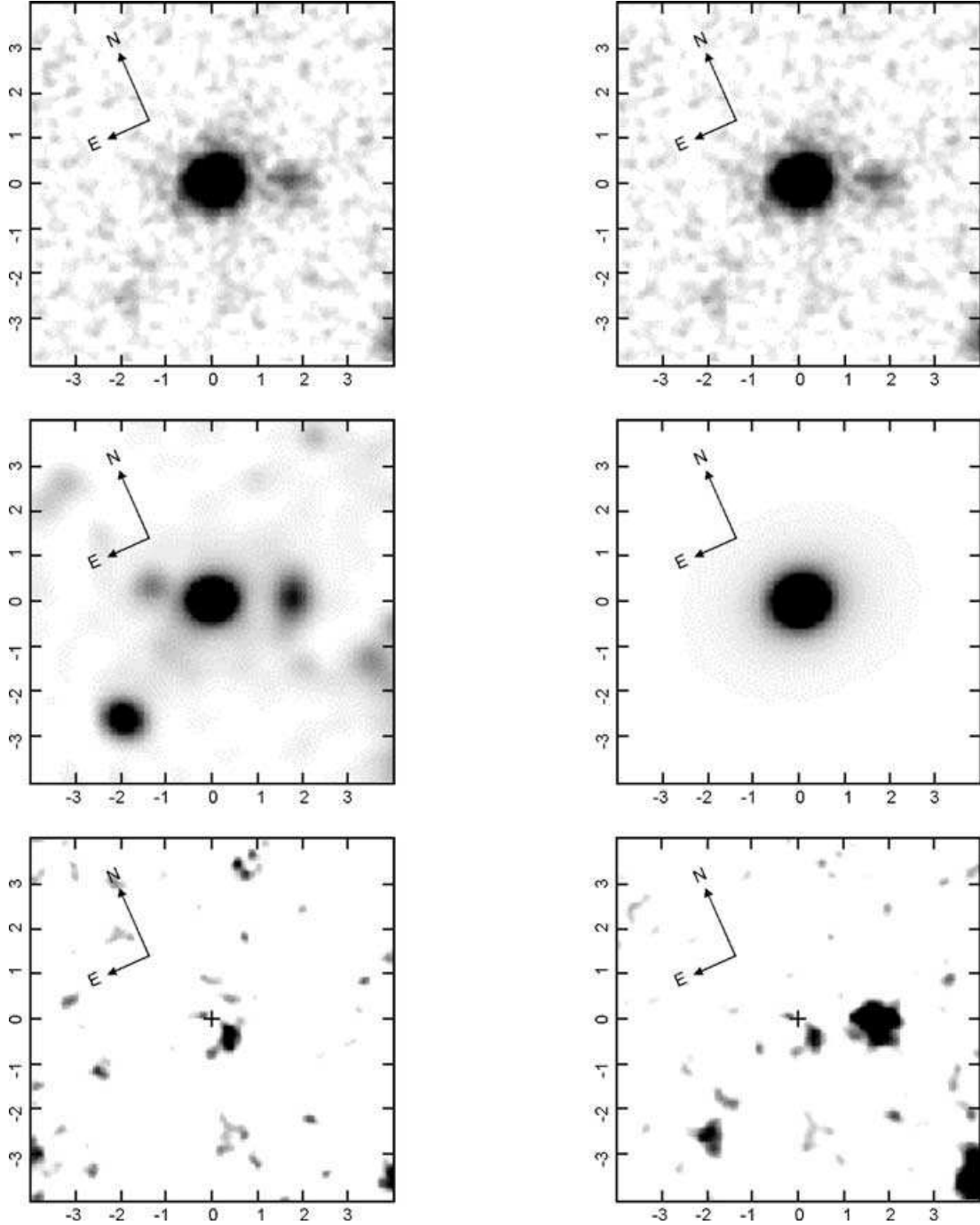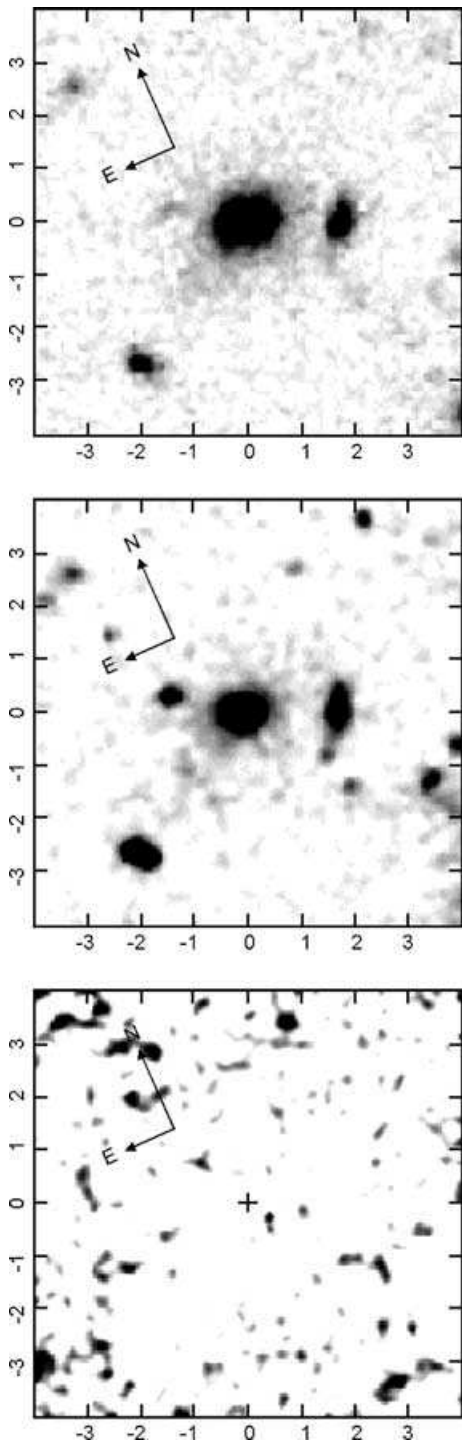
Figure 2. Subtraction of the $z_{ph} \simeq 1$ elliptical 3−586.0 from the Subaru K' image. The left-hand column shows the result of doing this using the *HST* WFPC2 F814W image of the same field. The top-left panel shows an 8×8 arcsec^2 postage stamp extracted from the Subaru image, centred on 3−586.0. The centre-left panel shows the same region, as imaged by the *HST* in the F814W filter, after convolution with a Gaussian of FWHM 0.57 arcsec. The bottom-left panel shows the residual image which results from subtracting the middle (F814W) image from the top (K') image after scaling both (background-subtracted) images to the same peak pixel value. The residual image has been smoothed with a Gaussian of FWHM 0.2 arcsec, and the cross marks the position of the centroid of 3−586.0 prior to subtraction. The right-hand column shows the result of doing this by fitting and subtracting the best-fitting de Vaucouleurs model of the K' light from 3−586.0. The top-right panel again shows the K' postage stamp. The centre-right panel shows the best-fitting elliptical galaxy model for 3−586.0, after convolution with 0.6-arcsec seeing (this model has an axial ratio of 1.28, a position angle of 85° east of north, and a half-light radius of 3.0 kpc). The bottom-right panel shows the residual image which results from subtracting the middle (model) image from the top (observed K') image. Again the residual image has been smoothed with a Gaussian of FWHM 0.2 arcsec, and the cross marks the centroid of 3−586.0 prior to subtraction.

4 NEAR-INFRARED IMAGE ANALYSIS

The Subaru K' image of the field shown in the top panel of Fig. 2 contains no obvious new candidate identification for HDF 850.1

over and above those present in the *HST* WFPC2 optical images as discussed in Section 2. However, because of the extreme depth of this image, and the fact it has been taken from the ground (albeit in excellent conditions, with a seeing disc FWHM of 0.6 arcsec),

the objects in the vicinity of HDF 850.1 appear considerably more extended than in the corresponding *HST* images. In particular, near-infrared emission from the $z \simeq 1$ elliptical $3-586.0$ is detectable out to an angular radius of $\simeq 1.5$ arcsec, and thus covers a significant region of the image within which the true identification of HDF 850.1 could potentially lie. We therefore decided to attempt to remove the light of $3-586.0$ from the K' image. This was done in two independent ways: first by subtracting an appropriately blurred and scaled version of the F814W image of the field, and second by fitting and removing a model representation of the elliptical from the K' image. As described below, these two alternative approaches yielded reassuringly similar results. We have also performed a similar analysis on the *HST* NICMOS Camera-3 F160W image of the HDF (Dickinson et al., in preparation), and find that this yields a marginal *H*-band detection at the same position (to within <0.1 arcsec) as the K' detection.

4.1 Subtraction of the F814W image from the K′ image

The K' image was interpolated onto the same pixel scale as the drizzled F814W image (0.04 arcsec), and then 8×8 arcsec^2 postage-stamp images were extracted at both wavelengths, centred on the fitted centroid of the elliptical $3-586.0$. The F814W image was then convolved with a Gaussian, scaled to the same central peak height as the K' image, and subtracted from it. The FWHM of the convolving Gaussian was varied until optimally clean subtraction of $3-586.0$ from the residual image was achieved. The optimum FWHM was 0.57 arcsec which, when added in quadrature to the intrinsic width of the *HST* F814W point spread function, makes good sense given the rms seeing of 0.6 arcsec determined from the full K' image of the HDF.

This process is summarized in Fig. 2 (left-hand column), which shows the K' image, the convolved F814W image, and the residual image. The small cross in the residual image marks the position of the centroid of $3-586.0$. It can be seen that the brightest source in this pseudo $K - I$ residual flux-density image is a small source, of visible angular extent $\simeq 0.5-0.7$ arcsec, lying 0.55 arcsec distant from the projected centre of $3-586.0$.
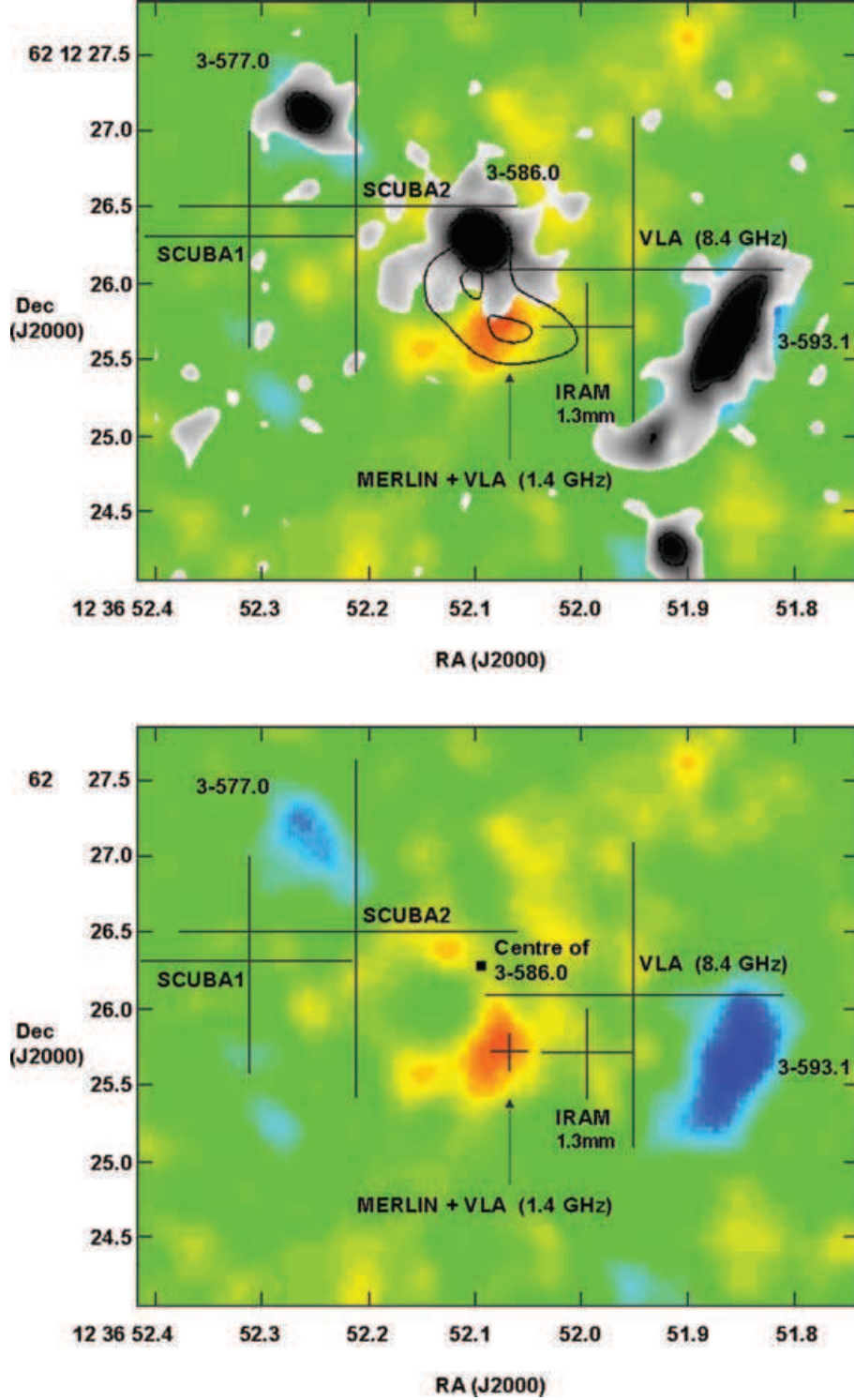
4.2 Subtraction of a model elliptical from the K′ image

A model elliptical galaxy was fitted to the original 0.1-arcsec pixel Subaru image of $3-586.0$ using a two-dimensional modelling code originally developed for modelling quasar host galaxies (McLure, Dunlop & Kukula 2000), incorporating 0.6-arcsec seeing. This model elliptical was then simply subtracted from the image to produce a second, alternative residual map of the field which was then interpolated on to 0.04-arcsec pixels for ease of comparison with the pseudo $K - I$ image discussed in the previous subsection.

This process is also summarized in Fig. 2 (right-hand column), which shows the raw K' image, the image of the best-fitting de Vaucouleurs model of $3-586.0$, and the residual image. All objects detected in the K' image other than $3-586.0$ are obviously still present in this residual image, but the one new object revealed by this model subtraction process is once again a small source, of visible angular extent $\simeq 0.5-0.7$ arcsec, lying 0.55 arcsec distant from the projected centre of $3-586.0$.

4.3 Subtraction of the F814W image from the NICMOS F160W image

The drizzled F160W image of the HDF (Dickinson et al., in preparation) was interpolated onto the same pixel scale as the drizzled

Figure 3. Subtraction of the $z \simeq 1$ elliptical $3-586.0$ from the *HST* NICMOS F160W image using a smoothed version of the *HST* WFPC2 F814W image of the same field. The top panel shows an 8×8 arcsec^2 postage stamp extracted from the NICMOS image, centred on $3-586.0$. The data have been 'drizzled' onto a pixel scale of 0.04 arcsec, for ease of comparison with the WFPC2 data. The centre panel shows the corresponding F814W image, after convolution with a Gaussian of FWHM 0.19 arcsec. The bottom panel shows the residual image which results from subtracting the middle (F814W) image from the top (F160W) image after scaling both images to the same peak pixel value. The residual image has been smoothed with a Gaussian of FWHM 0.12 arcsec, and the cross marks the centroid of $3-586.0$.

Figure 4. Upper panel: the pre-existing optical-to-radio information on HDF 850.1 from Fig. 1 (with the new MERLIN+VLA 1.4-GHz detection illustrated by the contours plotted at 8.5, 1.5 × 8.5, 2 × 8.5 μJy beam^{-1} etc.) overlaid on the $K - I$ colour image of the field discussed in Section 5.1. Lower panel: the same image, but this time with the grey-scale representation of the *HST* WFPC2 image removed, and the MERLIN+VLA contours replaced by a cross marking the formal position of (and 1σ uncertainty in) the brightest component of the 1.4-GHz source. This image makes it clear that, not only is the position of HDF 850.1K consistent with that of the MERLIN+VLA detection, but that, given the ≃0.1 arcsec uncertainty in the radio position, HDF 850.1K is the only plausible identification in the field.

F814W image (0.04 arcsec), and then 8 × 8 arcsec^2 postage-stamp images were extracted at both wavelengths, centred on the fitted centroid of the elliptical 3−586.0. The F814W image was then convolved with a Gaussian of FWHM 3.5 pixels (to degrade it to a resolution comparable with that of the F160W image), scaled to the same central peak height as the F160W image, and subtracted from it. The result of this process was not as clean as that achieved using the K' image. In particular, it produced a region of oversubtraction

around the centroid of 3−586.0 (at a radius ≃ 0.1–0.2 arcsec), possibly due to the difference between the Gaussian-convolved WFPC2 PSF and the more Airy disc-like NICMOS PSF. However, attempts to resolve this problem using convolution with the F160W PSF predicted by the TINY TIM software did not produce any significant improvement, suggesting that the problem could be an artefact of the drizzling algorithm. The resulting residual image should therefore be regarded with some caution. Nevertheless, as shown in Fig. 3 (which shows the NICMOS F160W image, the convolved F814W image, and the residual image), the brightest source in the central region of this pseudo $H − I$ residual flux-density image lies in exactly the same position, and has the same basic shape (i.e. extended along the same position angle) as the source revealed by the analysis of the K' image discussed above and illustrated in Fig. 2.

Further confidence in the security of the detection of the galaxy counterpart of HDF 850.1 in the Subaru K' image is provided by the fact that many of the *less* significant objects seen in the lower-left panel of Fig. 2 are confirmed as real in the completely independent NICMOS 160W image shown in the bottom panel of Fig. 3. Specifically, the objects seen at coordinates (0.7, 3.2), (−2.5, −1.2) and (−3.9, −3) in the lower panel of Fig 2 are all confirmed as real in the lower panel of Fig. 3, as indeed are the three very faint objects near the NE orientation indicator (the top one of which appears to be deblended in the NICMOS image). The NICMOS image contains some additional peaks, as expected given its higher resolution, and greater sensitivity for blue objects, but in terms of the K' detected objects the level of agreement is impressive.

5 RESULTS

5.1 Discovery of HDF 850.1K, the faint extremely red galaxy counterpart of the submm source HDF 850.1

The detection of a new source 0.55 arcsec distant from 3−586.0 in the bottom-right panel of Fig. 2 shows that it is genuinely due to an excess of K-band flux density, rather than to some defect in the F814W image. Furthermore, its presence in the bottom-left panel of Fig. 2 demonstrates that it is not simply an artefact of the model-fitting process due to, for example, the failure of a smooth elliptical model to describe the galaxy 3−586.0 adequately. Moreover, the similarity of this object in these two alternative residual images ($K − K_{model}$ and $K − I$) means that this object must be undetected in the F814W image.

To quantify the significance of this new K detection we performed aperture photometry on both the alternative residual images described above. To quantify the significance of its non-detection in the I band, we also performed aperture photometry at the same position in a residual F814W image, produced by fitting and subtracting a two-dimensional elliptical model to the F814W image of 3−586.0 (note that the validity of performing aperture photometry on the $K − I$ image is underpinned by the non-detection in the I-band image itself). To obtain an estimate of its $H − K$ colour we performed aperture photometry on the residual NICMOS F160W image shown in the bottom panel of Fig. 3, centred on the position of the K' detection.

The results of this photometry are given in Table 1. In summary, this new object (which we hereafter call HDF 850.1K) is a faint, but clearly significant (≃8σ) detection at K, with $K = 23.5 ± 0.2$, and is an extremely red galaxy (ERG), with $I − K > 5.2$ and $H − K = 1.4 ± 0.35$.

As can be seen from Table 1, the faintness of HDF 850.1K means that its K magnitude has to be based on measurements made through

Table 1. Near-infrared-to-radio photometry of HDF 850.1.

Band	Flux/Magnitude	Method/Source
K	$24.20 ± 0.1$	$0.5''$ diameter, $K − F814$
K	$24.55 ± 0.1$	$0.5''$ diameter, $K − model$
K	$23.40 ± 0.13$	$1.0''$ diameter, $K − F814$
K	$23.85 ± 0.13$	$1.0''$ diameter, $K − model$
K	$23.6 ± 0.25$	$1.0''$ diameter, adopted average
K	$23.4 ± 0.25$	$1.0''$ diameter, seeing corrected
$H − K$	$1.4 ± 0.35$	$0.5''$ diameter, seeing corrected
$I − K$	>5.2 $2σ$	$0.5''$ diameter, seeing corrected
$S_{450\mu m}$	<21 $3σ$ mJy	SCUBA; Hughes et al. (1998)
$S_{850\mu m}$	$7.0 ± 0.4$ mJy	SCUBA; Hughes et al. (1998)
$S_{1.3mm}$	$2.2 ± 0.3$ mJy	IRAM; Downes et al. (1999)
$S_{1.35mm}$	$2.1 ± 0.5$ mJy	SCUBA; Hughes et al. (1998)
$S_{8.4GHz}$	$7.5 ± 2.2$ μJy	E. Richards, priv. comm.
$S_{1.4GHz}$	<23 $3σ$ μJy	VLA; Richards (1999)
$S_{1.4GHz}$	$16 ± 4$ μJy	Merlin+VLA; this paper

relatively small software apertures (0.5–1.0 arcsec). There is no evidence that HDF 850.1K is significantly more extended than the 0.6-arcsec seeing disc in the sense that, correcting for the effects of seeing, the 0.5-arcsec measurement is certainly consistent with the 1.0-arcsec aperture measurement. However we cannot rule out the possibility that, given imaging of sufficient depth, HDF 850.1K might prove to be as extended as the K-band identification of Lockman850.1 reported by Lutz et al. (2001) (for which the 3-arcsec diameter aperture magnitude is 1.6 mag brighter than the 1-arcsec diameter aperture magnitude).

After clockwise rotation of the images shown in Fig. 2 to align with the RA and Dec coordinate system, a colour version of the residual $K − I$ image was combined with the information presented in Fig. 1, along with the MERLIN+VLA contours discussed in Section 3.2, to produce the combined image shown in the upper panel of Fig. 4. The accurate alignment of the residual colour image with Fig. 1 is aided by the negative images of 3−557.0 and 3−593.1 present in the former.

Relative to the centre of 3−586.0, the centroid of HDF 850.1K lies $0.2 ± 0.08$ arcsec west, and $0.5 ± 0.08$ arcsec south of the elliptical galaxy. Use of the accurate (50 mas rms) reference frame established from matching the MERLIN and *HST* images of the HDF then yields a position for HDF 850.1K of (J2000)

RA $12^h 36^m 52^s.072 ± 0^s.015$, Dec $+ 62° 12' 25''.75 ± 0''.1$.

Given the IRAM PdB position for HDF 850.1, and the well-documented fact (see Hughes et al. 1998; Downes et al. 1999) that none of the other plausible optical/IR counterparts (3−586.0, 3−593.1 or 3-593.2) appear to have estimated redshifts consistent with that estimated for HDF 850.1, it seems highly probable that HDF 850.1K is indeed the long-sought galaxy counterpart of the brightest SCUBA source in the HDF. This probability is obviously further increased by the fact that this object is an ERG, with a colour very similar to that which has been found for other, successful SCUBA source identifications (e.g. Lutz et al. 2001; Ivison et al. 2000, 2001; Smail et al. 1999; Frayer et al. 2000). However, perhaps most impressive of all, as illustrated in the lower panel of Fig. 4, is the essentially exact astrometric coincidence of HDF 850.1K with the tentative detection of HDF 850.1 in the combined MERLIN+VLA 1.4-GHz image, discussed above in Section 3.2, which yields a new radio position for HDF 850.1 accurate to 0.1 arcsec. The astrometric information for the various detections of HDF 850.1 as a function of frequency is summarized in Table 2.

Table 2. Positions of the detections of HDF 850.1 (see Fig. 4).

Band	RA (J2000)	Dec (J2000)
850 μm(1)	12^h 36^m $52.32^s \pm 0.10^s$	$62°$ $12'$ $26.3'' \pm 0.7''$
850 μm(2)	12^h 36^m $52.22^s \pm 0.10^s$	$62°$ $12'$ $26.5'' \pm 0.7''$
1.3 mm	12^h 36^m $51.98^s \pm 0.04^s$	$62°$ $12'$ $25.7'' \pm 0.3''$
1.4 GHz	12^h 36^m $52.060^s \pm 0.015^s$	$62°$ $12'$ $25.67'' \pm 0.07''$
K	12^h 36^m $52.072^s \pm 0.015^s$	$62°$ $12'$ $25.75'' \pm 0.1''$

The probability that HDF 850.1K is the correct identification of HDF 850.1 is quantified and discussed in more detail in Section 6.1, while the possible effects of lensing by 3−586.0 are discussed in Section 6.2. In order to inform this discussion, however, we first consider what can be learned about 3−586.0 from the optical-infrared image analysis presented here, and also calculate what new constraints can be placed on the estimated redshift of HDF 850.1 incorporating its new detection at 1.4 GHz.

5.2 Properties of the elliptical galaxy 3−586.0

As outlined in the Introduction, the galaxy 3−586.0 is already known to be a relatively quiescent, red elliptical with a credible estimated redshift of $z_{ph} = 1.1 \pm 0.1$ (Fernández-Soto et al. 1999). As part of the analysis presented here we have fitted a two-dimensional de Vaucouleurs model to the new ground-based K-band, and existing *HST V*- and *I*-band images of this galaxy. The results of this modelling are summarized in Table 3, where it can be seen that the half-light radius (r_e) depends on wavelength to a degree that is entirely consistent with the colour gradients exhibited by other well-studied ellipticals of comparable size.

We have used these results to estimate the velocity dispersion of this elliptical galaxy from the K-band fundamental plane (Mobasher et al. 1999). This was done in the following way. The observed K-band surface brightness of 3−586.0, at the half-light radius r_e, is $\mu_e = 20.5$. To convert this to a present-day surface brightness we have made the standard correction for cosmological dimming, incorporating a k-correction based on the typical rest-frame colour of a passively evolving elliptical ($J - K \simeq 1$), and assuming that between $z = 1$ and $z = 0$ this galaxy would be expected to dim by $\Delta K \simeq 0.5$ mag due to passive evolution. This latter assumption, equivalent to assuming a minimum level of evolution (i.e. a high formation redshift), is justified by the fact that, with observed colours of $I - K \simeq 4$ and $H - K \simeq 1$, it is clear that 3−586.0 is already a very passive and well-evolved galaxy close to the red envelope of galaxy evolution at $z \simeq 1$.

This calculation yields a rest-frame K-band surface brightness at r_e of $\mu_K = 18.7$, which converts to a mean surface brightness internal to r_e of $\langle \mu_K \rangle_e = 17.3$.

This number was then inserted into the relation between effective diameter (A_e), velocity dispersion (σ_v) and mean surface brightness

($\langle \mu_K \rangle_e$) derived by Mobasher et al. (1999) for the Coma cluster:

$$\log_{10}(A_e) = (1.38 \pm 0.26) \log_{10}(\sigma_v) + (0.3 \pm 0.02)\langle \mu_K \rangle_e - 7. \quad (1)$$

To obtain σ_v from this relation we calculated A_e for 3−586.0 by first converting the geometric average value of r_e given in Table 3 to the major axis value, doubling this and then transforming the result to the redshift of the Coma cluster ($z = 0.0231$). This yields a value of $A_e = 14.8$ arcsec.

The resulting estimate for the velocity dispersion of 3−586.0 is $\sigma_v = 146$ km s^{-1}, with an rms uncertainty of ± 29 km s^{-1}, which we calculated directly from the data for the Coma cluster provided by Mobasher et al. (1999).

This new estimate for the velocity dispersion of 3−586.0 is somewhat lower than the value previously estimated by Hogg et al. (1996). However, this earlier estimate was based purely on the Faber–Jackson relation, and did not allow for the effects of passive evolution.

5.3 The estimated redshift of the submm source

As discussed in Sections 2 and 3, compared with most other submm selected sources, the SED of HDF 850.1 is well sampled from the radio to FIR wavelengths. The upper panel of Fig. 5 shows the observed long-wavelength SED of HDF 850.1, normalized to its flux density at 850 μm. The shape of this SED can be used to determine the redshift probability distribution of the source. A Monte Carlo photometric redshift method has been developed (Hughes et al. 2002; Aretxaga et al. 2003) to also take into account constraining prior information such as the number counts of submm galaxies, the favoured evolutionary model of the submm population, and the amplification and clustering properties of a certain field. We assume that the SEDs of submm galaxies are well represented by 20 SEDs of local starbursts, ultraluminous infrared galaxies (ULIRGs) and AGN, all of which are well sampled in the radio–FIR regime to allow the reliable fitting of physically motivated functional relationships. The Monte Carlo technique yields the probability of producing the colours and flux densities of the submm galaxy under study at any given redshift, and thus provides us with the whole redshift probability distribution and not with just the first and second moments of the distribution, as popular maximum-likelihood techniques do.

This Monte Carlo redshift estimation technique places the most likely redshift of HDF 850.1 at $z_{est} = 4.1$ with a 68 per cent confidence interval of $3.5 \leqslant z_{est} \leqslant 4.6$ and a 90 per cent confidence interval of $3.0 \leqslant z_{est} \leqslant 5.1$. The redshift probability distribution is clearly consistent with earlier claims that locate HDF 850.1 at $z \geqslant 2.5$ (Hughes et al. 1998; Downes et al. 1999). The lower panel of Fig. 5 shows the redshift probability distributions found under different assumptions (details about the calculations are given in Aretxaga et al. 2003). Different lines correspond to different adopted evolutionary models of the submm population and possible lensing amplifications. The thick solid line corresponds to an unlensed scenario, and the thick dashed line to a lensed scenario where HDF

Table 3. Properties of the elliptical galaxy 3−586.0. Magnitudes were determined through an aperture of diameter 3 arcsec. Half-light radii assume $H_0 = 70$ km s^{-1} Mpc^{-1}, $\Omega_m = 0.3$, $\Omega_\Lambda = 0.7$. Velocity dispersion was estimated from the K-band fundamental plane (see Section 5.2).

RA (J2000)	Dec (J2000)	z	Magnitude	Scalelength r_e	velocity dispersion
12^h 36^m $52.101^s \pm 0.014^s$	$62°$ $12'$ $26.27'' \pm 0.1''$	1.1 ± 0.1	$K = 19.39 \pm 0.03$	3.0 kpc (at K)	146 ± 29 km s^{-1}
			$H = 20.40 \pm 0.05$	3.0 kpc (at H)	
			$I = 23.40 \pm 0.05$	3.3 kpc (at I)	
				4.0 kpc (at V)	
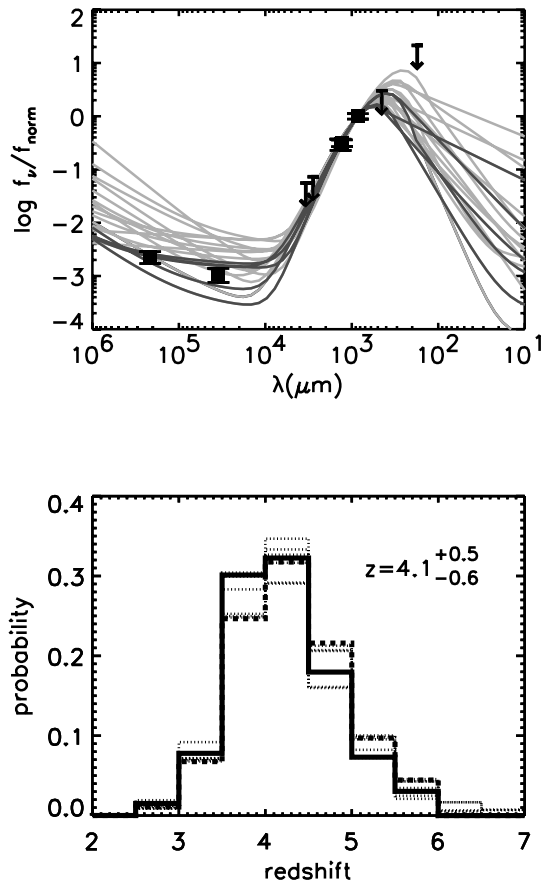
Figure 5. Results from the Monte Carlo photometric redshift estimation. Upper panel: SED of HDF 850.1 normalized to 850 μm, where squares are detections with superimposed 1σ error bars, and arrows indicate 3σ upper limits. The lines represent the SEDs of local starbursts, ULIRGs and AGN used in the calculation, redshifted to $z = 4.1$. Dark grey lines are SEDs compatible at a 3σ level with the SED of HDF 850.1, and light grey lines are SEDs that are not compatible within the 3σ level. Lower panel: redshift probability distributions derived for HDF 850.1. Different lines correspond to different adopted evolutionary models and amplification factors (see Aretxaga et al. 2003, for details). The thick solid line represents an unlensed scenario for a given evolutionary model, and the thick dashed line represents the corresponding lensed scenario. The mode of the redshift distribution and the 68 per cent confidence interval are indicated within the panel for the unlensed model. The lensed scenario yields an indistinguishable result.

850.1 is amplified by a factor of 3 (see Section 6.2). The results are almost independent of the adopted evolutionary model of the submm population and the lensing amplification of HDF 850.1 considered. Lensed models produce a minor transfer of probability from redshifts $z_{est} < 4$ to redshifts $z_{est} > 4.5$, as the likelihood of detecting fainter, higher-redshift sources with compatible colours is increased. However, the most probable redshift in the lensed scenarios is still basically the same, i.e. $z_{est} = 4.2$.

6 DISCUSSION

6.1 Robustness of the submm source identification HDF 850.1 K

6.1.1 Statistical association with the IRAM source

To estimate the statistical confidence with which this newly discovered faint ERO can by identified with the SCUBA source, we

first ignore the new radio information and simply add HDF 850.1K to the list of possible identifications for the 1.3-mm detection of HDF 850.1 considered by Downes et al. (1999). As illustrated in the lower panel of Fig. 4, the distance from the IRAM position to HDF 850.1K is 0.65 arcsec. The number density of galaxies with $K < 23.5$ is $\simeq 0.02$ arcsec^{-2} (Maihara et al. 2001). Consequently, the raw Poisson probability of finding HDF 850.1K so close to the IRAM position is $P_0 = 0.03$. As discussed by Downes et al. (1986) (see also Dunlop et al. 1989; Serjeant et al. 2002), however, this number needs to be corrected for the different ways that objects with this a posteriori Poisson probability could be found down to the limiting magnitude of the available data. Using the corrected number counts from table 3 of Maihara et al. (2001), the cumulative surface density of objects down to K = 25.5 is 0.07 arcsec^{-2}. So, for an adopted search radius around the IRAM source of 1 arcsec, the corrected probability that this is a chance coincidence is P = 0.09.

It is interesting to consider how this compares with the statistical probability that the elliptical $3-586.0$ lies so close to the IRAM source by chance. In this case, using the *I*-band *HST* data, we get a range of values depending on whether we use the catalogueof Williams et al. (1996) (W96), the SExtractor catalogue (www.stsci.edu/ftp/science/hdfsouth/catalogs.html), or the shallower Barger et al. (1999a) catalogue (B99). The raw Poisson probabilities of this coincidence calculated from these three different catalogues are $P_0 = 0.07$ (W96), 0.03 (Sextractor) and 0.01 (B99). If we again adopt a search radius of 1 arcsec around the IRAM source, the corrected probabilities become $P = 0.16$, 0.09 and 0.03 respectively. The probabilities for $3-593.1$ are somewhat higher and, as already noted, $3-577.0$ lies outside any reasonable search radius from the IRAM position.

Thus, ignoring the radio data we can conclude that the probability that HDF 850.1K lies so close to the IRAM source position by chance is $\simeq 5$ per cent, and that this 2σ result is comparable to the statistical significance of the IRAM+$3-586.0$ association. If, as has been argued above, $3-586.0$ can be rejected as a potential SCUBA identification on the grounds of estimated redshift, we can conclude that HDF 850.1K is the most likely counterpart for the IRAM source as revealed by all optical and near-infrared imaging undertaken to date.

Qualitatively, this identification seems all the more likely because it is an ERG ($I - K > 5.2$, $H - K \simeq 1.4$), given that several of the most secure SCUBA identifications have comparable colours (e.g. Lutz et al. 2001; Smail et al. 1999; Dey et al. 1999; Ivison et al. 2000, 2001). However, factoring this observation into the statistical calculation is difficult because the surface density of ERGs is not properly determined at this depth. Specifically, while *K*-band number counts reaching $K = 23$ have been published in three papers (Moustakas et al. 1997; Bershady, Lowenthal & Koo 1998; Maihara et al. 2001), in only one of these are deep *I*-band data also presented (Moustakas et al. 1997), and in this case the authors find no galaxy with $I - K > 5$ and $K > 23$ in a 2-arcmin^2 field.

Alexander et al. (2001) define 'very red objects' (VROs) as having $I - K > 4$, and report a cumulative number density of 1500 ($+250$, -250) deg^{-2} to $HK' = 20.4$, and 6100 ($+2800$, -2000) deg^{-2} to $K = 22$. So, down to $K = 22$ we can calculate that the probability of finding a VRO 0.65 arcsec from the IRAM position by chance (even adopting a source density of 8900 deg^{-2}) is $P_0 = 0.001$. Clearly this number will be increased by going to increased depth in *K*, but it will decrease if the redder threshold $I - K > 5$ appropriate to the current study is adopted. In fact, these two factors will roughly cancel out, as can be seen from an extrapolation of the results of Smith et al. (2002), who estimate the number densities of ERGs (in $R - K \geqslant 5.3$

and $R - K \geqslant 6.0$ subsamples) down to K = 21.5. Extrapolating the results of their redder subsample, as appropriate for HDF 850.1K, yields a very rough estimate of ~ 0.001 ERG arcsec^{-2} at K = 23.5, which translates to a probability of $P_0 \sim 0.001$ that such an object would be found 0.65 arcsec from the IRAM position by chance.

6.1.2 Statistical association with the new 1.4-GHz detection

The statistical probabilities calculated above are already reasonably compelling. However, we have not yet made use of the new 1.4-GHz MERLIN+VLA detection to refine the expected position and search radius for the optical/IR counterpart.

To do this we first calculate the probability that this 1.4-GHz MERLIN+VLA source is indeed the same source as detected by IRAM at 1.3 mm. In fact, since the angular separation of these two sources is only 0.56 arcsec (see Fig. 4, lower panel), and the surface density of radio sources down to $S_{1.4\,\mathrm{GHz}} > 17$ μJy is only $\simeq 0.0009$ arcsec^{-2}, the Poisson probability of such a chance coincidence transpires to be only $P_0 = 0.0009$.

We can therefore safely assume that the 1.4-GHz source is indeed the mm/submm source, and therefore that the MERLIN+VLA 1.4-GHz detection offers the most accurate available position for HDF 850.1. If we now recalculate the probability that HDF 850.1K is a chance coincidence with HDF 850.1 we find a raw Poisson probability of $P_0 = 0.0009$, corrected to $P = 0.008$ if we adopt a 3σ search radius of 0.3 arcsec. This is a compellingly small number, which would only become smaller if we were able to factor in reliably the prior probability that the object is an ERG.

We conclude by noting that the 3σ search radius from the MERLIN+VLA position does not now extend to include the centroid of 3−586.0 (see Fig. 4), and so this object can now be excluded as a possible identification without recourse to arguments based on redshift estimates for both sources. Of course, the fact that 3−586.0 has eventually turned out *not* to be a feasible identification on astrometric grounds in a sense lends credence to the pre-existing redshift-estimate argument.

However, despite its rejection as a possible identification, it still remains the case that 3−586.0 lies surprisingly close to HDF 850.1 on the sky (at the 2σ level), a statistical result that merits a physical explanation. The most likely explanation is that HDF 850.1 has been gravitationally lensed by 3−586.0, a possibility that we explore and quantify below in Section 6.2.

6.1.3 Optical–infrared constraints on the redshift of HDF 850.1K

Having established that HDF 850.1K is statistically highly likely to be the true galaxy counterpart of the submm source, it remains to consider whether, unlike 3−586.0, its optical–infrared photometric redshift estimate is at least consistent with that derived for the submm source from the longer-wavelength data in Section 5.3.

Given that the available information on HDF 850.1K consists of only a K magnitude, an approximate $H - K$ colour, and a limit on $I - K$ colour, it is obviously impossible to make an accurate estimate of its redshift. However, it is still worth exploring what constraints can be placed on its redshift under the assumption that its intrinsic properties are not unlike those of low-redshift ULIRGs. This assumption is of course debatable, and indeed there is some evidence that the near-infrared to ultraviolet properties of local ULIRGs do not quite correspond to the red colours of the submm population (local ULIRGs are in general bluer than the ERGs associated with
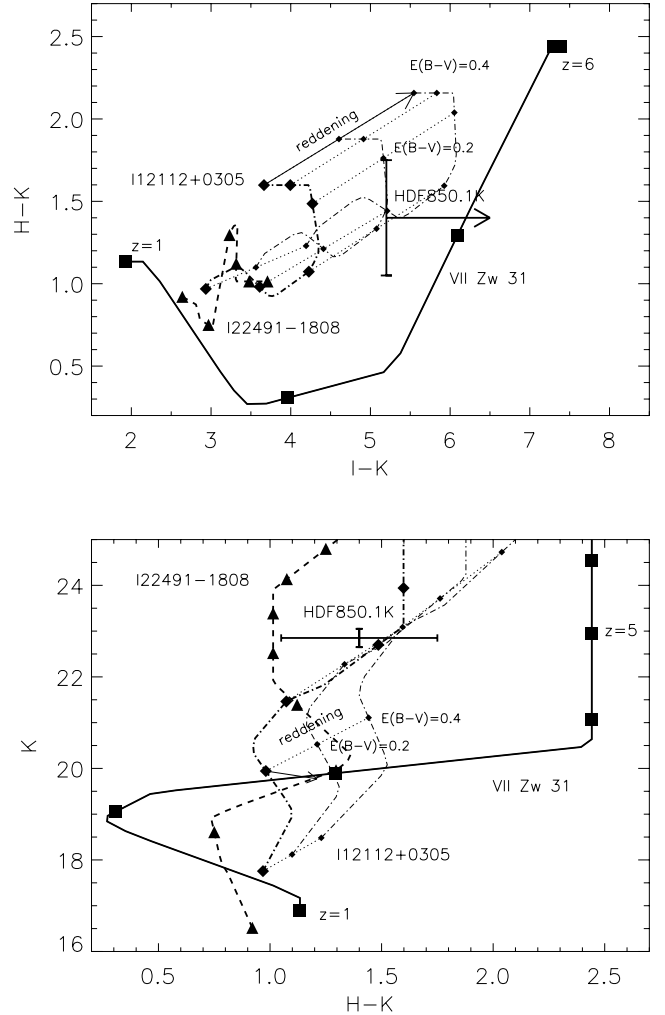
Figure 6. $H - K$ versus $I - K$, and K versus $H - K$ diagrams showing the predicted tracks of 5-mJy 1.2-mm sources with increasing redshift, taking the local ULIRGs I12112+0305, I22491−1808 and VII Zw 31 (thick lines) as analogues. The symbols represent the position in the track of each galaxy at $\Delta z = 1$ steps, starting from $z = 1$ at the bottom left of each figure. The effect of an increase in reddening is shown by the parallel curves to the right of I22491−1808, in thin lines and small symbols. HDF 850.1K appears near the centre of each figure, with its $H - K$ and $I - K$ colours, and (appropriately scaled) K magnitude indicated by 1σ error bars.

submm galaxies; Dannerbauer et al. 2002). Nevertheless, in the absence of a good set of UV–optical–IR templates to determine the photometric redshift of HDF 850.1K, we have used the local sample of ULIRGs to look for constraints on its redshift, independently of the redshift associated with the radio–mm–FIR source (Aretxaga et al. 2003).

The upper panel of Fig. 6 shows the $H - K$ versus $I - K$ colours of three local ULIRGs with available UV–optical colours (Trentham, Kormendy & Sanders 1999) when they are placed at different redshifts. At $z > 4.7$, the predicted I magnitude is calculated based on extrapolations from the rest-frame 1450-Å measurements, the shortest-wavelength at which these ULIRGs have been detected, and thus this redshift regime should be interpreted with caution. The colour offsets produced by increasing the amount of reddening $E(B - V) = 0.2, 0.4$ according to a typical starburst extinction law (Calzetti et al. 2000) are shown for I12112+0305, and are similar for

the other ULIRGs. The colours of HDH850.1K can be reproduced within the 1σ confidence interval by VII Zw 31 at $z = 2.8$–3.2 ($z = 2.6$–6.0 within 3σ), by I12112+0305 at $z = 3.3$–4.0 allowing for a $E(B - V) = 0.2$ increased extinction ($z = 3.3$–4.5 within 3σ), and by I22491−1808 at $z = 3.5$–4.0 allowing for a $E(B - V) = 0.4$ increased extinction ($z = 4.7$–6.0 within 3σ). Increasing the amount of extinction over these values can result in the accommodation of lower redshift ranges, as shown by the parallel tracks of I12112+0305 in Fig. 6. Similarly, de-reddening values of $E(B - V) \leqslant 0.5$ can accommodate higher redshift intervals ($z < 6$) for VII Zw 31.

Recently, Dannerbauer et al. (2002) produced a diagnostic diagram to estimate the redshifts of mm-galaxies based on the K magnitude of their IR counterparts, taking a local sample of ULIRGs as templates. Their method provides a complementary constraint on the redshift interval compatible with the optical–IR observations of HDF 850.1K. The lower-panel of Fig. 6 shows the K versus $H - K$ magnitude–colour relationship that the local ULIRG sample describes when located at different redshifts. Following Dannerbauer et al. (2002), the K-band magnitudes are derived from scaled UV–optical–IR–mm SEDs that reproduce 5-mJy sources at 1.2 mm, and HDF 850.1K is, therefore, accordingly scaled to $K = 22.85 \pm 0.20$.

Disregarding reddening corrections, the only ULIRG compatible with the $H - K$, $I - K$ colours and K-band magnitude of HDF 850.1K within a 3σ confidence level is VII Zw 31 at $z_{\rm ph} = 4.7$–5.2. However, a small increase $E(B - V) = 0.2$ in the amount of reddening of I12112+0305 can reproduce the colours of HDF 850.1K within a 1σ confidence interval at $z_{\rm ph} = 3.3$–3.5, and within a 3σ confidence interval at $z_{\rm ph} = 3.0$–3.8. For I22491−1808, the same is true using additional extinction corrections $E(B - V) = 0.4$, at $z_{\rm ph} \approx 3.8$ within a 1σ interval, and at $z_{\rm ph} \approx 3.4$–4.0 within a 3σ interval.

In summary, if placed at $z_{\rm ph} = 3.0$–5.2, the template local ULIRGs could reproduce the $H - K$, $I - K$ colours and K magnitudes of HDF 850.1K within the 3σ confidence interval. The probability that the redshift of the submm source is in the $z_{\rm ph} = 3.0$–5.2 regime is 90 per cent based on its radio–submm–FIR colours (Section 5.3). Therefore, although the derivation of a reliable optical–infrared photometric redshift for HDF 850.1K is not possible given the present optical–infrared data, this analysis does at least show that these data are completely consistent with the redshift interval derived in Section 5.3.

6.2 Gravitational lensing

6.2.1 The HDF 850.1 + 3−586.0 system

One striking aspect of the new proposed identification of HDF 850.1 is its proximity to the elliptical 3−586.0. With a low photometric redshift ($z_{\rm ph} = 1.1 \pm 0.1$), this elliptical was considered a poor candidate identification by Hughes et al. (1998). These authors nevertheless recognized that a $z \simeq 1$ elliptical such as 3−586.0 had a low probability of aligning with a SCUBA source by chance, and they proposed that gravitational lensing by the foreground elliptical could have enhanced this probability. We now revisit this possibility in the light of our improved knowledge of the identification of HDF 850.1 and the properties of 3−586.0.

The main features of the putative lens–source system are as follows. The observed separation of lens and main image is 0.55 arcsec, but there is no suggestion of a counter-image. This statement does not assume that any counter-image would be exactly opposite the main image; Fig. 2 shows that there is no other significant image in

the general vicinity. Based on the noise within 0.5-arcsec diameter photometric apertures on the K' image, we adopt a 2σ limit for a counter-image of $K > 26$, which implies an upper limit of 0.26 for the flux ratio between any counter-image and the main image. This lack of evidence for strong lensing constrains a combination of the mass of 3−586.0 and the redshift of HDF 850.1; in the following discussion, we assume a standard $\Omega = 0.3$, $k = 0$ geometry.

The simplest lens model to consider for 3−586.0 is a singular isothermal sphere, for which the only parameter is the angular radius of the Einstein ring:

$$\theta_{\rm E} = \left(\frac{\sigma_{\rm v}}{186 \text{ km s}^{-1}} \right)^2 \frac{D_{\rm LS}}{D_{\rm S}} \quad \text{arcsec,} \qquad (2)$$

where $\sigma_{\rm v}$ is the velocity dispersion of the lensing galaxy, and $D_{\rm LS}$ and $D_{\rm S}$ are the angular diameter distances to the lens and the source respectively (e.g. Peacock 1999). For an observed separation θ between lens and main image, multiple imaging is predicted if $\theta < 2\theta_{\rm E}$, with total amplification $A = 2\theta_{\rm E}/(\theta - \theta_{\rm E})$, and a flux ratio between counter-image and main image of $(2\theta_{\rm E}/\theta) - 1$. The lack of an obvious counter-image suggests that we cannot be very far into the strong-lensing regime; the 2σ limit is a counter-image with flux density 0.26 times that of the main image, which corresponds to a total amplification $A = 3.4$. Together with the observed radius of the main image at 0.55 arcsec from the centre of 3−586.0, this yields the following constraint on the Einstein radius:

$$\theta_{\rm E} < 0.35 \text{ arcsec;} \quad A_{\rm max} = 3.4. \qquad (3)$$

This allows a redshift-dependent limit to be set on the velocity dispersion of 3−586.0, as shown in Fig. 7 (upper panel). If the photometric redshift indication for HDF 850.1 is at all realistic, the velocity dispersion of 3−586.0 cannot exceed about 160 km s^{-1} in this model.

A more realistic model will have a finite core to the mass distribution. We assume that 3−586.0 is baryon-dominated in the centre, so that the observed $r^{1/4}$ profile gives the bend-angle profile directly, up to a free M/L. With this assumption the bend angle has a broad peak at 0.9-arcsec radius, falling to half this value at 0.15 arcsec. We connect this to the isothermal sphere model by assuming that the bend angle remains constant beyond 0.9 arcsec, and we use this asymptotic value to give an effective velocity dispersion to the lens, which is most conveniently quoted as the Einstein radius that corresponds to a singular model with the same asymptotic bend angle. For this non-singular profile, the onset of multiple lensing is more abrupt: additional images first form with divergent amplification via caustic-crossing, at which point the amplification of the main image is $A = 6.4$. The limit on the lens properties now changes to

$$\theta_{\rm E} < 0.47 \text{arcsec;} \quad A_{\rm max} = 6.4. \qquad (4)$$

This permits a slightly more massive lens: up to $\sigma_{\rm v} = 178$ km s^{-1} for $z_{\rm S} = 4.1$, as compared to a limit of $\sigma_{\rm v} = 154$ km s^{-1} for the singular model with this source redshift. Given the velocity dispersion estimate of $\sigma_{\rm v} = 146 \pm 29$ km s^{-1} for 3−586.0, inferred from the K-band fundamental plane in Table 3, it seems that 3−586.0 must be causing significant lensing amplification. This is shown in the lower panel of Fig. 7, which shows the likelihood evaluated over the plane of source redshift and total amplification (assuming the non-singular model), using the estimate of the velocity dispersion (assuming the error distribution to be Gaussian in $\ln\sigma$) and the radio–submm source redshift estimate of $z_{\rm est} = 4.1 \pm 0.5$ (assuming the error distribution to be Gaussian in z). Integrating the likelihood values up to $A_{\rm max} = 6.4$ yields a median amplification of 3.6, with a 95 per cent confidence lower limit of 1.7.
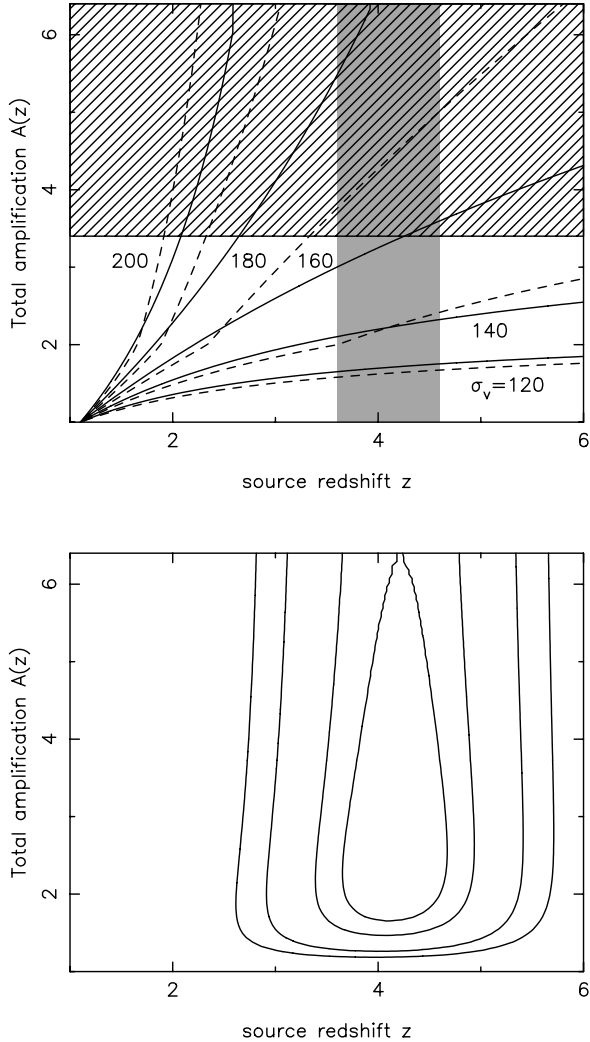
Figure 7. The effect of gravitational lensing on HDF 850.1. The upper panel shows predicted total lensing magnification as a function of source redshift for different assumed values of the velocity dispersion (σ_v) of the lensing $z \simeq 1$ elliptical 3−586.0. The dashed lines show the case of a singular isothermal sphere; the solid lines show the more realistic case in which the mass model has a core (see text). The 2σ limit on any counter-image is a flux density 0.26 times that of the main image; this corresponds to a total amplification $A < 3.4$ for the singular model (hatched area), or $A < 6.4$ for the model with a core. If the photometric redshift indication for HDF 850.1 is at all realistic, the velocity dispersion cannot exceed about 160 km s^{-1}, consistent with the velocity dispersion of $\sigma_v = 146 \pm 29$ km s^{-1} deduced independently from the infrared fundamental plane (see Section 5.2 and Table 3). The lower panel shows likelihood contours for the total lensing magnification of HDF 850.1 and its redshift, taking account of the estimated velocity dispersion for the foreground elliptical, the limits on any counter-image, plus the photometric redshift and its uncertainty. Likelihood contours are plotted at the usual positions for one-parameter 68 per cent confidence and two-parameter confidence values of 68 per cent, 95 per cent, and 99 per cent (i.e. offsets in ln L of 0.5, 1.15, 3.0 and 4.6). We see that it seems inevitable that HDF 850.1 has been subject to significant lensing amplification: a 95 per cent confidence lower limit of a factor 1.7. Note that we cannot rule out the alternative possibility of stronger on-axis lensing, in which a slight ellipticity of the lens would break the symmetry between main and counter-image. This would require a more massive lens, with $\sigma_v \simeq 200$ km s^{-1}.

For a more massive lens, constrained to yield one image at 0.55-arcsec radius, significant counter-images are generally predicted. There are, however, two ways of evading the conclusion that the maximum lensing amplification is 6.4. The first is to consider the possibility that the observed image is in fact not the principal image: if the true position of HDF 850.1 is actually on the opposite side of 3−586.0, the observed image could be the result of a merging pair of secondary images produced when the source crosses the outer caustic. The amplification for this situation can be divergent. This seems improbable, however, since the lens would need to be unrealistically massive in order to produce secondary images at 0.55 arcsec ($\theta_E = 2.8$ arcsec). A more realistic alternative with extreme amplification results if we relax the assumption of a circularly symmetric lens, in accord with the measured axial ratio of 1.28 for 3−586.0. This has little effect on the lensing properties at moderate amplifications, but greatly changes the high-amplification limit. An inner caustic opens up, and it is possible to achieve divergent amplification with large image flux ratios if the source is placed close to this caustic. For this option, the lens mass has to be such that the observed critical line passes through the image radius of 0.55 arcsec. For a circular lens, this would require $\theta_E = 0.57$ arcsec, or $\sigma_v = 198$ km s^{-1} for $z_S = 4.1$.

Finally, we should consider whether it is legitimate to model the lens as a single component. If 3−586.0 were to lie in a rich cluster with a constant-density core just below the critical surface density, strong lensing effects could arise with a much less massive galaxy, as in, for example, the case of cB58 (Seitz et al. 1998), which has some similarities with the present situation. However, cB58 was found towards a pre-selected X-ray-luminous cluster; even at $z = 1.1$, it is clear that nothing remotely as massive exists around 3−586.0. Assuming a source redshift of $z_{est} = 4.1$, the critical surface density at 3−586.0 is 7.2×10^{14} h M$_\odot$ Mpc^{-2}; the most massive known clusters at $z = 0.8$ have surface densities similar in magnitude to the the critical value of interest here (Clowe et al. 1998), but these are rare systems, which would be extremely prominent on data of the HDF depth.

Such systems would also be very easily detected at X-ray wavelengths in the deep Chandra imaging of this field. In fact, the 1-Msec Chandra image centred on the HDF revealed six extended sources in the full 16×16 arcmin field (Bauer et al. 2002). These can be used to obtain a conservative upper limit on any cluster emission in the vicinity of HDF 850.1, which lies in the most sensitive part of the X-ray image. The two faintest extended sources from Bauer et al. (2002) have an X-ray flux density of $\simeq 3 \times 10^{-19}$ Wm^{-2} (0.5 − 8 keV). There is no evidence for any X-ray emission in the vicinity of HDF 850.1, which, assuming $z \simeq 1$ for a high-redshift cluster containing 3−586.0, leads to an upper limit on cluster X-ray luminosity of $L_X < 2 \times 10^{35}$ W. This corresponds to the X-ray luminosity of a weak group, $\simeq 100$ times fainter than the *ROSAT* and EMSS $z \simeq 1$ clusters discussed by Clowe et al. (1998).

In summary, there are two possibilities regarding gravitational lensing of HDF 850.1, assuming it to lie at $z_{est} = 4.1$: (i) a lens with $\sigma_v < 178$ km s^{-1} would imply that there is no multiple imaging, and that the total amplification is moderate ($A \simeq 3$); (ii) for σ_v close to 200 km s^{-1}, there is also the possibility of extreme nearly on-axis lensing, in which the amplification is not constrained, and could plausibly be more than 10 times larger. The velocity dispersion estimate of $\sigma_v = 146 \pm 29$ km s^{-1} for 3−586.0 favours the former model, but does not completely rule out the on-axis case. One may suspect that $K \simeq 23.5$ is already so faint that cB58-like amplifications of order 30 are implausible, but in the absence of other evidence

it is best to consider the a priori probabilities of these outcomes, as discussed below.

6.2.2 Estimated prevalence of lensing within the submm source population

What are the implications of HDF 850.1 for the occurrence of lensing in other SCUBA sources? It is important to understand whether this is an isolated rare event, or if lensing needs to be taken into account in interpreting the data on all bright SCUBA sources (see also Chapman et al. 2002).

The expected amplification distribution is $P(>A) = \tau/A^2$, so we need an estimate of the lensing optical depth, $\tau(z)$. For a source at $z_{est} = 4.1$, this is $\tau = 0.12$ on the assumption that the galaxy population at $z \simeq 1$ is unchanged from that at $z = 0$ (e.g. Peacock 1982). Note that the optical depth is not sensitive to the exact lens model, and depends mainly on the total density of mass in systems of above critical surface density. Neglecting evolution means that $\tau = 0.12$ is probably an overestimate. Figures about a factor of 4 lower are obtained from calculations based on evolving dark-matter haloes (e.g. Perrotta et al. 2003). However, because these estimates neglect halo substructure, they are almost certainly too low. The correct figure is unlikely to be far from $\tau = 0.1$, so the intrinsic probability of strong ($A > 2$) lensing is only about 2 per cent. This is boosted by amplification bias: if the slope of the counts is $dN/d\ln S \propto S^{-\beta}$, the biased lensing probability is

$$P(>A) = \frac{2}{2-\beta}\frac{\tau}{A^{2-\beta}}. \tag{5}$$

For counts with the observed near–Euclidean slope of $\beta = 1.5$, this raises the probability to $P(A > 3) = 2.3\tau \simeq 0.2$. The probability of extreme amplification is lower, but here a power-law approximation to the counts is inadequate. If we adopt the count model from equation (25) of Peacock et al. (2000), we obtain a biased probability $P(A > 30) \simeq 0.006$. Together with the higher velocity dispersion needed for $3-586.0$ in the on-axis case, this strengthens the case for single-image lensing with a moderate amplification $A \simeq 3$ in the case of HDF 850.1. The observation of such an amplification in one of the first bright submm sources from a blank-field survey is consistent with our simple probability calculations, which indicate that a substantial fraction (perhaps of order one-fifth) of the high-redshift SCUBA sources should be affected by lensing amplifications of this order (Blain 1996; Blain, Moller & Maller 1999).

It should be possible to test this prediction once deep radio and infrared follow-up imaging of large, unbiased blank-field SCUBA surveys (such as the '8-mJy' survey; Scott et al. 2002) has been completed. For now the best we can say is that a lensed fraction of this order does not seem unreasonable. There is good evidence that, in a few cases, SCUBA sources have been significantly lensed by an intervening galaxy $\simeq 1$–2 arcsec distant from the true identification, based on radio or K-band imaging (Smail et al. 1999; Frayer et al. 2000). However, in at least one of these cases the lensing galaxy is associated with a foreground cluster used to boost the sensitivity of the SCUBA survey, (Smail et al. 1999) and thus the likelihood of such a lensing system may well be substantially greater than in blank-field SCUBA surveys.

Indeed, in contrast to HDF 850.1, none of the three other best-studied SCUBA sources selected from unbiased, blank-field surveys shows any evidence of having been lensed by an intervening galaxy (CUDSS14A – Gear et al. (2000); Lockman850.1 – Lutz et al. (2001); ELAISN2850.2 – Dunlop (2001a)). Moreover, this is also true for the three bright mm sources recently discussed by Dannerbauer et al. (2002). It thus seems clear that significant lensing is *not* in general responsible for the bright submm/mm source population. On the other hand, lensing of a significant minority of the sources detected in the '8-mJy' survey may well offer an explanation for the apparent correlation between the SCUBA sources, and galaxies at relatively modest redshift found in the ELAIS N2 and HDF fields by Almaini et al. (in preparation).

6.3 Cosmic star-formation history revisited

We conclude this discussion by considering how the new information we now possess on HDF 850.1 impacts on the original estimation of dust-enshrouded star-formation density at high redshift performed by Hughes et al. (1998). The three main issues to consider are (i) the improved confidence in radio–FIR photometric redshifts which follows from the discovery of HDF 850.1K; (ii) revised constraints on the plausibility that HDF 850.1 and other SCUBA sources are powered by AGN rather than starbursts; and (iii) appropriate corrections for gravitational lensing in the light of this study.

6.3.1 Estimated redshifts

One important consequence of the discovery of HDF 850.1K is that it provides renewed confidence that the high SCUBA-source redshifts inferred from radio–far-infrared SED fitting should be trusted, even when the SCUBA source itself appears (at first, or even second, sight) to be associated with a galaxy of surprisingly modest redshift. It also reinforces the importance of very deep radio, mm and infrared imaging for SCUBA-source follow-up prior to attempting spectroscopy of candidate identifications within the original SCUBA error circle (e.g. Barger et al. 1999b).

If one trusts the radio–far-infrared SED-based redshift estimates, then current evidence suggests a median redshift $z_{est} \simeq 3$ for the bright SCUBA galaxy population (Dunlop 2001b; Smail et al. 2000), with the substantial majority of SCUBA sources lying at $z_{est} > 2$. Equally, the relative ease with which several other bright SCUBA sources have been identified compared to HDF 850.1 suggests that the majority probably lie at $z_{est} < 4$ (although this study reinforces the need for excellent astrometric precision and calibration of the follow-up data). Thus, it still seems reasonable to follow Hughes et al. (1998) and assume an approximate redshift range $2 < z_{est} < 4$ for calculating the contribution made by submm sources to star-formation density.

6.3.2 X-ray constraints on AGN activity

Evidence continues to grow that SCUBA and Chandra/XMM sources, while perhaps correlated on large scales, are rarely coincident (e.g. Fabian et al. 2000; Bautz et al. 2000; Hornschemeier et al. 2000; Barger et al. 2001a, 2001b; Almaini et al. 2003). As discussed in the Introduction, for the case of HDF 850.1, the nearest detected X-ray source lies $\simeq 5$ arcsec south-west of the SCUBA source. However, the extreme depth of the 1-Msec Chandra image of the HDF, coupled with the fact that we now possess such an accurate position for HDF 850.1, makes it of interest to calculate what *limits* can be placed on the presence of an AGN in this source.

We have deduced 3σ upper limits on the X-ray flux density of HDF 850.1 using the Bayesian method of Kraft, Burrows & Burrows (1991). This yields a limit of $< 4 \times 10^{-20}$ Wm^{-2} in the soft band (0.5–2 keV), and $< 3 \times 10^{-19}$ Wm^{-2} in the hard band (2–8 keV)

Table 4. Inferred 3σ upper limits on X-ray luminosity (L_X), and black-hole mass (M_{bh}) for HDF 850.1, assuming a range of absorbing columns (n_H).

n_H/m^{-2}	L_X/W	$M_{bh}/M_\odot$
10^{27}	4×10^{36}	4×10^6
10^{28}	6×10^{36}	6×10^6
10^{29}	1.5×10^{37}	1.5×10^7
Comp thick (1 per cent scat)	3×10^{38}	3×10^8

The resulting submm–to–X-ray ratios yield a spectral index $\alpha_{sx} > 1.4$. Reference to fig. 4 of Almaini et al. (2003) demonstrates that such a value is entirely consistent with a starburst, but means that an AGN cannot be powering the submm emission unless the obscuring column is Compton-thick with a negligible scattered fraction ($\ll 1$ per cent).

What limits can we place on the luminosity/black hole mass of any AGN present in HDF 850.1? This clearly depends on the level of absorption assumed. If we assume no absorption, than adopting z =4 yields a limiting X-ray luminosity of $L < 3 \times 10^{36}$W, comparable to the output of a weak Seyfert galaxy. Using a standard bolometric correction (a factor $\simeq 12$), the assumption of Eddington-limited accretion yields an upper limit on black-hole mass of 3×10^6 M$_\odot$.

If we consider a range of absorbing columns, the upper limits on the inferred X-ray luminosity and black-hole mass are as summarized in Table 4. Thus it can be seen that unless the absorbing column is Compton-thick, the limiting black-hole mass is $\simeq 10^7$ M$_\odot$.

6.3.3 *Impact of gravitational lensing*

Although the results of this study indicate that the flux density of HDF 850.1 has almost certainly been boosted by gravitational lensing, the inferred magnification factor is relatively modest, $\simeq 2-3$. There is also no evidence to support the existence of a similar lensing system for any of the other HDF SCUBA sources. This is not surprising since it is the brightest source uncovered that is statistically most likely to be significantly lensed, and the occurrence of one case of lensing within the five sources reported by Hughes et al. (1998) is certainly consistent with the estimates of lensing prevalence given above.

It therefore seems reasonable to simply scale down the intrinsic submm luminosity of HDF 850.1 by a factor of 3, for the purpose of recalculating the total comoving star-formation density of the five SCUBA sources in the HDF. This produces a reduction of $\simeq 30$ per cent in the estimate of comoving star-formation density reported by Hughes et al. (1998).

7 CONCLUSION

This study has provided a particularly compelling demonstration of the importance of ultra-deep near-infrared and radio imaging for the successful identification of even the brightest of submm selected sources. The contrast between the submm and optical views of the HDF could hardly be more striking, with the galaxy counterpart of the brightest submm source in this field transpiring to be one of the faintest and reddest objects ever uncovered at near-infrared/optical wavelengths. At such imaging depths, subarcsec astrometric accuracy is clearly crucial if an unambiguous identification is to be secured.

It is obviously unrealistic to expect that multifrequency data of this depth and quality will be easily achieved for large samples of bright submm sources. It is therefore worth briefly revisiting what would have been concluded about HDF 850.1 without the enormous investment of observing time made with the IRAM PdB interferometer, VLA+Merlin, and most recently Subaru. As discussed at the beginning of this paper, on the basis of statistical association one would have concluded that HDF 850.1 should be identified with the $z_{ph} \simeq 1$ elliptical galaxy 3−586.0. Alternatively, given the growing evidence that SCUBA galaxies are ERGs, and given the uncertainty in raw SCUBA-source positions, another apparently plausible (and statistically likely) conclusion would be that HDF 850.1 should be identified with the nearby (5 arcsec distant) ERG, which is also the nearest obvious Chandra and VLA source (VLA 3651+1221). The former error would lead to the conclusion that HDF 850.1 lies at relatively modest redshift, and that submm–radio SED-based redshift estimation cannot be trusted. The latter error would lead to the conclusion that HDF 850.1 is an AGN.

In fact, of course, neither of these previously possible conclusions can now be viewed as tenable, and we find that HDF 850.1 does indeed appear to be a violently star-forming galaxy at $z_{est} \simeq 4$, which could never be discovered via Lyman-break selection techniques.

REFERENCES

Alexander D. M., Brandt W. N., Hornschemeier A. E., Garmire G. P., Schneider D. P., Bauer F. E., Griffiths R. E., 2001, AJ, 122, 2156
Almaini O. et al., 2003, MNRAS, 338, 303
Aretxaga I., Hughes D. H., Chapin E. L., Gaztanaga E., Dunlop J. S., 2003, MNRAS, 342, 759
Barger A. J., Cowie L. L., Trentham N., Fulton E., Hu E. M., Songaila A., Hall D., 1999a, AJ, 117, 102 (B99)
Barger A. J., Cowie L. L., Smail I., Ivison R. J., Blain A. W., Kneib J.-P., 1999b, AJ, 117, 2656
Barger A. J., Cowie L. L., Richards E. A., 2000, AJ, 119, 2092
Barger A. J., Cowie L. L., Mushotzky R. F., Richards E. A., 2001a, AJ, 121, 662
Barger A. J., Cowie L. L., Steffen A. T., Hornschemeier A. E., Bradnt W. N., Garmire G. P., 2001b, ApJ, 560, L23
Bauer F. E. et al., 2002, AJ, 123, 1163
Bautz M. W., Malm M. R., Baganoff F. K., Ricker G. R., Canizares C. R., Brandt W. N., Hornschmeier A. E., Garmire G. P., 2000, ApJ, 543, L119
Bershady M. A., Lowenthal J. D., Koo D. C., 1998, ApJ, 505, 50
Blain A. W., 1996, MNRAS, 283, 1340
Blain A. W., Moller O., Maller A., 1999, MNRAS, 303, 423
Calzetti D., Armus L., Bohlin R. C., Kinney A. L., Koornneef J., Storchi-Bergmann T., 2000, ApJ, 533, 682
Carilli C., Yun M., 1999, ApJ, 513, L13

Carilli C., Yun M., 2000, ApJ, 530, 618

Chapman S. C., Smail I., Ivison R. J., Blain A. W., 2002, MNRAS, 335, L17

Clowe D., Luppino G. A., Kaiser N., Henry J. P., Gioia I. M., 1998, ApJ, 497, L61

Dannerbauer H., Lehnert M., lutz D., Tacconi L., Bertoldi F., Carilli C., Genzel R., Menten K., 2002, ApJ, 573, 473

Dey A., Graham J. R., Ivison R. J., Smail I., Wright G. S., Liu M. C., 1999, ApJ, 519, 610

Downes A. J. B., Peacock J. A., Savage A., Carrie D. R., 1986, MNRAS, 218, 31

Downes D. et al., 1999, A&A, 347, 809

Dunlop J. S., 2001a, in Lowenthal J. D., Hughes D. H., eds, Deep Millimetre Surveys. World Scientific Press, Singapore, p. 11

Dunlop J. S., 2001b, in van Bemmel I. M., Wilkes B., Barthel P., eds, FIRSED2000, New Astronomy Reviews, 45. Elsevier, Amsterdam, 609 (astro-ph/0101297)

Dunlop J. S., Peacock J. A., Savage A., Lilly S. J., Heasley J. N., Simon A. J. B., 1989, MNRAS, 238, 1171

Dunne L., Clements D. L., Eales S. A., 2000, MNRAS, 315, 115

Fabian A. C. et al., 2000, MNRAS, 315, L8

Fernández-Soto A., Lanzetta K. M., Yahil A., 1999, ApJ, 513, 34

Frayer D. T., Smail I., Ivison R. J., Scoville N. Z., 2000, AJ, 120, 1668

Garrington S. T., Muxlow T. W. B., Garrett M. A., 2001, in Schilizzi R. T., ed., Proc. IAU Symp. 205, Galaxies and their Constituents at the Highest Angular Resolutions. Kluwer, Dordrecht, p. 102

Gear W. K., Lilly S. J., Stevens J. A., Clements D. L., Webb T. M., Eales S. A., Dunne L., 2000, MNRAS, 316, L51

Hawarden T. G., Leggett S. K., Letawsky M. B., Ballantyne D. R., Casali M. M., 2001, MNRAS, 325, 563

Hogg D. W., Blandford R., Kundić T., Fassnacht C. D., Malhotra S., 1996, ApJ, 467, L73

Hornschemeier A. E. et al., 2000, ApJ, 541, 49

Hughes D. H. et al., 1998, Nat, 394, 241

Hughes D. H. et al., 2002, MNRAS, 335, 871

Ivison R. J., Smail I., Le Borgne J.-F., Blain A. W., Kneib J.-P., Bézecourt J., Kerr T. H., Davies J. K., 1998, MNRAS, 298, 583

Ivison R. J., Smail I., Barger A. J., Kneib J.-P., Blain A. W., Owen F. N., Kerr T. H., Cowie L. L., 2000, MNRAS, 315, 209

Ivison R. J., Smail I., Frayer D. T., Kneib J.-P., Blain A. W., 2001, ApJ, 561, L45

Kraft R. P., Burrows D. N., Nousek J. A., 1991, ApJ, 374, 344

Lawrence A., 2001, MNRAS, 323, 147

Lutz D. et al., 2001, A&A, 378, 70

Ma C. et al., 1998, AJ, 116, 516

McLure R. J., Dunlop J. S., Kukula M. J., 2000, MNRAS, 318, 693

Maihara T. et al., 2001, PASJ, 53, 25

Mobasher B., Guzmán R., Aragón-Salamanca A., Zepf S., 1999, MNRAS, 304, 225

Motohara K. et al., 2002, PASJ, 54, 315

Moustakas L., Davis M., Graham J. R., Silk J., Peterson B. A., Yoshii Y., 1997, ApJ, 475, 445

Muxlow T. W. B., Garrington S. T., Richards A. M. S., Richards E. A., Garrett M. A., Kellermann K. I., Alberdi A., 2000, in Conway J. E., Polatidis A. G., Booth R. S., Pihlstrom Y. M., eds, EVN Symp. 2000, Onsala Space Observatory. 133.

Peacock J. A., 1982, MNRAS, 199, 987

Peacock J. A., 1999, Cosmological Physics. Cambridge University Press, Cambridge

Peacock J. A. et al., 2000, MNRAS, 318, 535

Perrotta F., Magliocchetti M., Baccigalupi C., Bartelmann M., De Zotti G., Granato G. L., Silva L., Danese L., 2003, MNRAS, 338, 623

Richards E. A., 1999, ApJ, 513, L9

Richards E. A., Kellerman K. I., Fomalont E. B., Windhorst R. A., Partridge R. B., 1998, AJ, 116, 1039

Rowan-Robinson M., 2003, MNRAS, in press (astro-ph/0307529)

Scott S. et al., 2002, MNRAS, 331, 817

Seitz S., Saglia R. P., Bender R., Hopp U., Belloni P., Ziegler B., 1998, MNRAS, 298, 945

Serjeant S. et al., 2003, MNRAS, 344, 887

Smail I., Ivison R. J., Kneib J. P., Cowie L. L., Blain A. W., Barger A. J., Owen F. N., Morrison G. E., 1999, MNRAS, 308, 1061

Smail I., Ivison R. J., Owen F. N., Blain A. W., Kneib J.-P., 2000, ApJ, 528, 612

Smith G. P. et al., 2002, MNRAS, 330, 1

Trentham N., Kormendy J., Sanders D. B., 1999, AJ, 117, 2152

Williams R. E. et al., 1996, AJ, 112, 1335 (W96)

Zepf S. E., Moustakas L. A., Davis M., 1997, ApJ, 474, L1